Floral pigments and their perception by avian pollinators in three Chilean Puya species

Takayuki Mizuno

tmizuno@kahaku.go.jp

National Museum of Nature and Science: Kokuritsu Kagaku Hakubutsukan

Shinnosuke Mori

Faculty of Science and Technology, Keio University

Koutarou Sugahara

Bioorganic Research Institute, SUNTORY foundation for Life Sciences

Tomohisa Yukawa

National Museum of Nature and Science: Kokuritsu Kagaku Hakubutsukan

Satoshi Koi

Osaka University School of Science Graduate School of Science: Osaka Daigaku Daigakuin Rigaku Kenkyuka Rigakubu

Tsukasa Iwashina

National Museum of Nature and Science: Kokuritsu Kagaku Hakubutsukan

Research Article

Keywords: anthocyanins, Bromeliaceae, color turning, intermolecular co-pigmentation, vacuole pH

Posted Date: November 15th, 2023

DOI: https://doi.org/10.21203/rs.3.rs-3579433/v1

Version of Record: A version of this preprint was published at Journal of Plant Research on March 4th, 2024. See the published version at https://doi.org/10.1007/s10265-024-01531-6.

Abstract

The Chilean *Puya* species, *Puya coerulea* var. *violacea* and *P. chiliensis* bear blue and pale-yellow flowers, respectively, while *P. alpestris* considered to be their hybrid-derived species has unique turquoise flowers. In this study, the chemical basis underlying the different coloration of the three *Puya* species was explored. We first isolated and identified three anthocyanins: delphinidin 3,3',5'-tri-*O*-glucoside, delphinidin 3,3'-di-*O*-glucoside and delphinidin 3-*O*-glucoside; seven flavonols: quercetin 3-*O*-rutinoside 3'-*O*-glucoside, quercetin 3,3'-di-*O*-glucoside, quercetin 3-*O*-rutinoside, isorhamnetin 3-*O*-rutinoside, myricetin 3,3',5'-tri-*O*-glucoside, myricetin 3,3'-di-*O*-glucoside and laricitrin 3,5'-di-*O*-glucoside; and six flavones: luteolin 4'-*O*-glucoside, apigenin 4'-*O*-glucoside, tricetin 4'-*O*-glucoside, tricetin 3',5'-di-*O*-glucoside, tricetin 3'-*O*-glucoside and selagin 5'-*O*-glucoside from their petals. We also compared compositions of floral flavonoid and their aglycone among these species, which suggested that the turquoise species *P. alpestris* has an essentially intermediate composition between the blue and pale-yellow species. The vacuolar pH was relatively higher in the turquoise (pH 6.2) and pale-yellow (pH 6.2) flower species, while that of blue flower species was usual (pH 5.2). The flower color was reconstructed *in vitro* using isolated anthocyanin, flavonol and flavone at neutral and acidic pH, and its color was analyzed by reflectance spectra and the visual modeling of their avian pollinators. The modeling demonstrated that the higher pH of the turquoise and pale-yellow species enhances the chromatic contrast and spectral purity. The precise regulation of flower color by flavonoid composition and vacuolar pH may be adapted to the visual perception of their avian pollinator vision.

Introduction

Turquoise color development of flowers is rare in nature, and such the unique trait needs to be understood and discussed how it was acquired (Iwashina et al., 2015; Okitsu et al., 2018). *Puya alpestris* (Poepp.) Gay (Bromeliaceae), endemic to Chile (Schulte et al., 2010; Zizka et al., 2013), bears turquoise flowers. Anthocyanin, delphinidin 3,3',5'-tri-*O*-glucoside, flavones, apigenin 4'-*O*-glucoside and luteolin 4'-*O*-glucoside, and flavonols, myricetin 3,3',5'-tri-*O*-glucoside and myricetin 3-*O*-rutinoside 3',5'-di-*O*-glucoside have been reported as its flower pigments (Mizuno et al., 2021). Moreover, it has been revealed that the turquoise color expression is developed by co-expression of blue color due to intermolecular copigmentation between their anthocyanin and flavones, and pale-yellow color expression from the flavonols under relatively higher pH (Scogin and Freeman, 1984; Scogin, 1985; Mizuno et al., 2021).

Molecular phylogenetic studies of *Puya* have revealed that *P. alpestris* has a sister relationship with Chilean *Puya* species and suggested that the turquoise flowered species is derived from a hybrid between blue flowered *P. coerulea* Lindl. and/or *P. venusta*, (Baker) Phil., and pale-yellow flowered *P. chilensis* Molina and/or *P. gilmartiniae* G.S.Varad. & A.R.Flores (Jabaily and Sytsma, 2010). In addition, ecological studies of Chilean *Puya* species have showed the relationship between their avian pollinators and morphology and nectar characteristics of these flowers (Hornung et al., 2013). According to Hornung et al. (2013), blue flowered species *P. coerulea* and *P. venusta* are mainly visited by specialist hummingbirds, having highly concentrated nectar in relatively low volume and no sterile apex in the inflorescence. On the

other hand, *P. alpestris* and *P. chilensis* have lower nectar concentration in large nectar volume and sterile apexes, which are exclusively visited by generalist passerines (Hornung et al., 2013). These pollinators of the three *Puya* species include both visual sensory types, ultraviolet-sensitive (UVS) and violet-sensitive (VS) type (Ödeen and Håstad, 2010).

In this study, to understand the chemical basis in natural history of acquisition of the unique flower color trait, the flower pigments, anthocyanins, flavones and flavonol were isolated and identified from the flower of bluish *P. coerulea* var. *violacea*, turquoise *P. alpestris*, and pale-yellow *P. chilensis*. We then compared the flavonoid composition among these Chilean *Puya* species to examine the chemical factor lying on their different floral coloration. Color parameters of these *Puya* flowers were also evaluated based on the visual models of UVS- and VS-avian pollinators, using *in vitro* reconstructed flower colors. Moreover, we discussed the possibility of generation of the turquoise flowered species by interspecific hybridization between blue flowered and pale yellow flowered *Puya* species.

Results

Identification of the flavonoids.

Three anthocyanins (**1**–**3**), four flavonols (**4**–**7**) and three flavones (**8**–**10**) were isolated from the flowers of *P. coerulea* var. *violacea*. On the other hand, three flavonols (**11**, **12** and **14**) and three flavones (**13**, **15** and **16**) were isolated from the flowers of *P. chilensis*. Their chemical structures are shown in Figs. 1A and B, and Table 1.

The liquid chromatography-mass spectrometry (LC/MS) measurement of three anthocyanins exhibited molecular ion peaks at *m/z* 789 $[M]^+$ (**1**), 627 $[M]^+$ (**2**) and 465 $[M]^+$ (**3**). Fragment ion peaks corresponding to delphinidin were observed at *m/z* 303 $[M]^+$ for all of **1**–**3**. The UV–vis spectra of these anthocyanins showed the relatively high E_{440}/E_{max} values, 21–32%, meaning that the 5-hydroxyl group is free. In anthocyanin **3**, bathochromic shift of the λ_{max} was observed by addition of $AlCl_3$, showing the presence of *ortho*-dihydroxyl group in the B-ring. Finally, they were identified as delphinidin 3,3',5'-tri-*O*-glucoside (**1**, preternatin C5), delphinidin 3',5'-di-*O*-glucoside (**2**) and delphinidin 3-*O*-glucoside (**3**, myrtillin) by HPLC and TLC comparisons with the authentic samples. Compound **1** has been reported from the flowers of *P. alpestris* as the main pigment (Mizuno et al., 2021).

Compound **4** showed the peaks of deprotonated molecule at *m/z* 771 $[M - H]^-$ and fragment ions at *m/z* 625 $[M - H-146]^-$ and 303 $[M - H-162\times2 - 146]^-$ on LC/MS. UV spectral properties indicated that the aglycone of **4** has free 5-, 7- and 4'-hydroxyl groups. In nuclear magnetic resonance (NMR) spectrum, five aromatic proton signals at δ_H 8.01 (*d*, H-2'), 7.92 (*dd*, H-6'), 6.94 (*d*, H-5'), 6.45 (*brs*, H-8) and 6.19 (*brs*, H-6) appeared (Table 2). The attachment of glucose to 3- and 3'-positions of aglycone was determined by HMBC correlation between glucosyl anomeric proton signals at δ_H 5.04 and 4.97, and C-3 and C-3' signals at δ_C 134.2 and 146.5, respectively (Fig. S1). The β-pyranose form of the glucose was assigned by ^1H NMR and NOESY correlation (Fig. S2) (Markham and Geiger, 1994). Thus, **4** was identified as

quercetin 3-*O*-rhamnopyranosyl-(1→6)-glucopyranoside-3'-*O*-glucopyranoside. The compound has been reported from the seeds of *Fagopyrum tataricum* (L.) Gaertn. (Polygonaceae) (Wu et al., 2007).

The peaks of deprotonated **5, 6** and **7** occurred at *m/z* 625, 609 and 623 $[M - H]^-$, respectively. From the UV spectral properties, these compounds were compared by HPLC and TLC with authentic samples, and identified as quercetin 3,3'-di-*O*-glucoside (**5**), quercetin 3-*O*-rutinoside (**6**) and isorhamnetin 3-*O*-rutinoside (**7**).

The LC/MS of **8**, **9** and **10** showed the peaks at *m/z* 447 and 433 $[M + H]^+$ and 463 $[M - H]^-$, respectively. Compounds **8** and **9** were identified as luteolin 4'-*O*-glucoside (**8**) and apigenin 4'-*O*-glucoside (**9**) by UV spectral properties and HPLC and TLC comparisons with authentic samples. Compound **8** has been isolated and identified as copigment substance for blue expression from the flowers of *P. alpestris* (Mizuno et al., 2021). Compound **10** was characterized as tricetin 4'-*O*-glucoside by UV and NMR spectra analysis after acid hydrolysis.

LC/MS of **11** detected the peaks of deprotonated molecule at *m/z* 803 $[M - H]^-$ and three fragment ions at *m/z* 643 $[M + H - 162]^+$, 481 $[M + H - 162\times2]^+$ and 319 $[M + H - 162\times3]^+$, meaning that **11** is myricetin attached to 3 mol hexoses. UV spectral properties showed that **11** is myricetin glycosylated at the 3-, 3'- and 5'-positions. Finally, it was determined as myricetin 3,3',5'-tri-*O*-glucoside by HPLC and TLC comparisons with an authentic sample, which has been reported as pale-yellow pigment from the flowers of *P. alpestris* (Mizuno et al., 2021).

Compound **12** showed the peaks of deprotonated molecule at *m/z* 641 $[M - H]^-$ and fragment ions at *m/z* 481 $[M + H - 162]^+$ and 319 $[M + H - 162\times2]^+$ on LC/MS, showing that **12** is myricetin attached to 2 mol hexoses. UV spectral properties showed that 3- and 3'-positions of myricetin are glycosylated. In ^{1}H NMR spectrum, four aromatic proton signals, δ_H 7.63 (*d*, H-2'), 7.50 (*d*, H-6'), 6.41 (*d*, H-8) and 6.18 (*d*, H-6) appeared (Table 2). The attachment of the sugars to 3- and 3'-position of myricetin was determined by HMBC correlation between anomeric proton signals at δ_H 5.20 (*d*) and δ_H 4.87 (*d*) and C-3 and C-3' signals at δ_C 135.7 and δ_C 146.9, respectively (Fig. S3). The β-pyranose forms of the glucose were assigned by ^{1}H NMR and NOESY correlation (Fig. S4). Thus, **12** was identified as myricetin 3,3'-di-*O*-glucopyranoside. The compound has been found in the leaves of *Rhizophora mangle* (Rhizophoraceae) (Kandil et al., 2004).

LC/MS of **13** showed the peaks at *m/z* 627 $[M + H]^+$ and 625 $[M - H]^-$ and the fragment ion peak at *m/z* 311 $[M + H - 162\times2]^+$, suggesting that **13** is tricetin attached to 2 mol hexoses. UV spectral properties showed that the presence of free 7- and 4'-hydroxyl groups. In ^{1}H NMR spectrum, four aromatic proton signals, δ_H 7.63 (*brs*, H-2', 6'), 6.64 (*s*, H-3), 6.53 (*d*, H-8) and 6.18 (*d*, H-6) appeared (Table 3). The attachment of glucose to 3',5'-positions of tricetin was determined by HMBC correlation between glucosyl anomeric proton signal at δ_H 4.90 (2H, *d*) and C-3',5' signal at δ_C 146.9–147.0 (Fig. S5). The β-pyranose form of the glucose was assigned by ^{1}H NMR and NOESY correlation (Fig. S6). Thus, **13** was identified as

tricetin 3',5'-di-*O*-glucopyranoside. The compound has been reported from *Dacrycarpus dacrydioides* (Podocarpaceae) (Markham and Whitehouse, 1984).

Compound **14** showed the peaks of deprotonated molecule at *m/z* 655 $[M - H]^-$ and fragment ions at *m/z* 495 [M + H − 162] and 333 [M + H − 162×2] on LC/MS, suggesting that **14** is monomethoxylated myricetin attached to 2 mol hexoses. UV spectral properties were the same with those of **4**, that is, **14** is methoxylated and di-*O*-glycosylated at 3,3',5'-positions. In ^{1}H NMR spectrum, four aromatic proton signals, δ_H 7.73 (*d*, H-2'), 7.65 (*d*, H-6'), 6.46 (*d*, H-8) and 6.20 (*d*, H-6) appeared (Table 2). The methoxy proton signal was observed at δ_H 3.94 (*s*). The attachment of methoxy group to 3'-position of myricetin was determined by HMBC correlation between methoxy proton signal at δ_H 3.94 and C-3' carbon signal at δ_C 149.2 (Fig. S7 and S8). On the other hand, the attachment of hexose to 3,5'-positions of myricetin was determined by HMBC correlation between glucosyl anomeric protons at δ_H 5.36 and δ_H 4.89 and C-3 and C-5' signals at δ_C 135.7 and and δ_C 146.6, respectively (Fig. S7). The β-pyranose structure of glucose was assigned by ^{1}H NMR and NOESY correlation (Fig. S8). Thus, **14** was identified as laricitrin 3,5'-di-*O*-glucopyranoside. The compound has been reported from the aerial parts of *Medicago littoralis* Rhode. (Fabaceae) (Alessandra et al., 2010).

The LC/MS analysis of **15** detected the peaks at *m/z* 465 $[M + H]^+$ and 463 $[M - H]^-$. UV spectral properties indicated that **15** is a flavone having *orth*-dihydroxyl group in the B-ring. Five aromatic proton signals, δ_H 7.48 (*d*, H-2'), 7.20 (*d*, H-6'), 6.59 (*s*, H-3), 6.49 (*d*, H-8) and 6.21 (*d*, H-6) appeared in the NMR spectrum (Table 3). The attachment of glucose to 3'-position of aglycone was determined by HMBC correlation between glucosyl anomeric proton signal at δ_H 4.87 and C-3' signal at δ_C 147.8 (Fig. S9). The β-pyranose form of the glucose was assigned by ^{1}H NMR and NOESY correlation (Fig. S10). Thus, **15** was identified as tricetin 3'-*O*-glucopyranoside. The compound has been reported from the leaves of *Thuja occidentalis* L. and *Lathyrus pratensis* L. (Lamer et al., 1968; Reynauld et al., 1981)

Compound **16** showed the peaks at *m/z* 479 $[M + H]^+$ and 477 $[M - H]^-$ on LC/MS. UV spectral properties were identical with those of **13**. In ^{1}H NMR spectrum, five aromatic proton signals, δ_H 7.60 (H-2'), 7.32 (H-6'), 6.68 (*s*, H-3), 6.52 (*d*, H-8) and 6.21 (*d*, H-6) occurred (Table 3). Methoxy proton signal was observed at δ_H 3.97 and correlated with C-3' signal at δ_C 147.3 by HMBC, showing that a methoxy group is attached to 3'-position of the aglycone (Fig. S11). The glycosylation at 5'-position of the aglycone was determined by HMBC correlation between glucosyl anomeric proton at δ_H 4.90 and C-5' signal at δ_C 104.6. The pyranose form of the sugar was assigned by NOESY correlation (Fig. S12). Thus, **16** was identified as selagin 5'-*O*-glucopyranoside, which is an undescribed flavone (Buckingham J, Munasinghe V R N, 2015).

Flavonoid comparison among three Puya species

HPLC chromatograms of the extracts from three *Puya* species are shown in Fig. 1 and Table 1. Flavones **8** (16.1%) and **9** (8.3%) were detected as the main components of *P. coerulea* var. *violacea*. In pale yellow *P. chilensis*, flavonols **11** (23.1%) and **14** (13.2%), and flavone **16** (36.3%) were detected as the main

components. HPLC chromatogram showed that the turquoise flowers of *P. alpestirs* contain all of **8**, **9**, **11**, **14** and **16**; thus, *P. alpestirs* seems to have an intermediated characters between blue and pale-yellow *Puya* species.

The HPLC profiles of three *Puya* species were compared using a principal component (PC) analysis (Fig. 2). The proportion of variance was 0.6324 in first PC and 0.3079 in second PC. The 2-dimension scatter diagram of the PC analysis is shown in Fig. 2A. The content of anthocyanin **1** was the main factor having a positive effect on the first PC value. The second PC value was positively affected by **11** (myricetin 3,3',5'-tri-*O*-glucoside), **14** (laricitrin 3,5'-di-*O*-glucoside) and **16** (selagin 5'-*O*-glucoside). The locus of *P. coerulea* var. *violacea* was closer to that of *P. alpestris* (distance = 0.366) than of *P. chilensis* (distance = 1.092).

In addition, the scatter diagram excluding anthocyanin-derived factors is shown in Fig. 2B. The proportion of variance was 0.4690 in the first PC and 0.3600 in the second PC. The first PC value was influenced positively by the contents of **11** (myricetin 3,3',5'-tri-*O*-glucoside) and **16** (selagin 5'-*O*-glucoside), and negatively by those of **8** (luteolin 4'-*O*-glucoside) and **9** (apigenin 4'-*O*-glucoside). The distance between the loci of *P. coerulea* var. *violacea* and *P. alpestris* (0.970) and that of *P. chiliensis* and *P. alpestris* (0.965) were almost the same.

Aglycone analysis

The proportion of flavonol and flavone aglycones in the flower of three Chilean *Puya* species was examined by HPLC analysis of the products obtained by acid hydrolysis. Ten aglycones were detected in total (Fig. 3, Table S1). Among them, luteolin type flavones such as luteolin and chrysoeriol (37.5%), and tricetin type flavones (20.5%) including tricetin and selagin were the major flavonoids in *P. coerulea* var. *violacea*. In the extracts of *P. chilensis*, high proportions of tricetin (44.3%), and myricetin type flavonols, including myricetin and laricitrin (32.9%) were contained. In *P. alpestris*, luteolin type flavones (31.7%) including luteolin and chrysoeriol, and the myricetin type flavonols (23.7%) were contained as its major flavonoids. The proportion charts of the aglycones in respective species are shown in Fig. 3C, together with presumable flavonoid biosynthetic pathway (Fig. 3B).

Flower color analysis using absorption spectra

The visible absorption spectra of the blueish *P. coerulea* var. *violacea*, turquoise *P. alpestris*, and pale-yellowish *P. chilensis* are shown in Fig. 4A. The petal of *P. alpestris* exhibited the absorption maxima at 573, 614 and 678 nm, as reported in the previous report (Mizuno et al., 2021). Two absorption maxima were observed at 579 and 613 nm in the petal of *P. coerulea* var. *violacea*, indicating that the petal is blueish. On the other hand, absorption was mainly observed at 400–500 nm in the petal of *P. chilensis*. The spectral curve did not show any absorption peaks of carotenoids, whose absorption maxima are around ca. 400–500 nm (Zscheile et al., 1942). In addition, a small peak at 678 nm was observed in the petal of *P. chilensis*, which was presumed to be derived from chlorophylls (Mizuno et al., 2021).

In vitro reconstruction of flower colors

The pH values of the pressed petal juice of *P. coerulea* var. *violacea* and *P. chiliensis* were 5.2 and 6.2, respectively. The petal pH of *P. alpestris* is found to be 6.2 (Mizuno et al., 2021). The flower color was reconstructed with the characteristic pigments of three *Puya* species, **1**, **8** and **11**, and analyzed by reflectance spectra (Fig. 3B). The reconstruction was carried out as follows: the mixture of 0.07 mM **1** and 0.1 mM **8** (**1** + **8**) for *P. coerulea* var. *violacea*; the mixture of 0.07 mM **1**, 0.1 mM **8** and 0.1 mM **11** (**1** + **8** + **11**) for *P. alpestris*; and 0.1mM **11** (**11**) for *P. chiliensis* in two different pH buffers, 5.0 and 7.0. Buffer solutions of **1** + **8** in both pH reflected wavelengths corresponding to blue and red regions and appeared violet blue. The buffer solution of **1** + **8** + **11** at pH 7.0 had a similar reflectance to **1** + **8**; but the secondary peak was shifted to lower wavelength (around 500 nm) by addition of **11**, being turquoise in color. However, turquoise color was not expressed in pH 5.0, being dullish purple. The buffer solution of **11** at pH 7.0 appeared yellowish color, and its reflectance curve between 300–400 nm was different from the solution of pH 5.0.

Using these reflectance spectra, the color loci of each solution in the visual model of ultraviolet-sensitive (UVS) and violet-sensitive (VS)-avian species were modeled (Figs. 5 and 6). In the UVS-avian color space, the color loci of the bluish solutions of **1** + **8** at pH 5.0 and 7.0 were closely located, and displayed no significant difference in values of chromatic contrast (ΔS), achromatic contrast (ΔL) and spectral purity between the two pH. On the other hand, the pH had a larger effect for **11** and **1** + **8** + **11**, compared to **1** + **8**; the higher pH largely increased ΔS and spectral purity and decreased ΔL. In the VS-avian tetrahedral color spaces (Fig. 6E), although all color parameters followed the same tendency with those in the UVS color space, the effect of pH was relatively small.

Discussion

Three anthocyanins, seven flavonols and six flavones were isolated from the flowers of Chilean *Puya* species. The flavonoids in these species were composed of various aglycones, and many of them were glucosylated at the B-ring such as 3’,4’- and/or 5’-positions. Flavonoids including anthocyanins have been reported from the genus *Puya* (Scogin, 1985; Williams, 1978). In addition, delphinidin 3,3',5'-tri-*O*-glucoside and myricetin 3,3',5'-tri-*O*-glucoside have been isolated from the turquoise flowers of *P. alpestris* (Mizuno et al., 2021). Furthermore, various glycosides of myricetin, quercetin, laricitrin, isorhamnetin and apigenin have been detected by MS analysis of the meristem and leaves of *P. chiliensis* (Jiménez-Aspee, et al., 2018). Our data on the detail identification of flavonoids using NMR might contribute to the further chemotaxonomic, biological, and pharmaceutical study of the related species.

In this study, we showed the distribution of flavonoids in the flowers of three Chilean *Puya* species by HPLC (Fig. 1). From the result, we presumed that turquoise flowered *P. alpestris* contains both the compounds contained in blue flowered *P. coerulea* var. *violacea* and pale-yellow flowered *P. chilensis*. The relationship among three *Puya* species visualized in the scatter diagram by 2-dimension PC analysis (Fig. 2) showed that the presence of anthocyanin **1** significantly affected the first PC. The locus of *P. alpestris* was located closer to that of *P. coerulea* var. *violacea* than *P. chilensis*. In the PC analysis without anthocyanins, the first PC showed that *P. alpestris* is an intermediate position between *P. coerulea*

var. *violacea* and *P. chiliensis*. Meanwhile, the second PC value of *P. alpestris* was notably higher than the other two species, which may be accounted by the abundance of **8**, **9**, and **11**. It means that the flavonoid composition of *P. alpestris* tends to be intermediate between those of the other two species, but is characteristic.

Variation in the flower color is often associated with the flavonoid composition regulated through the biosynthesis pathway, which has been discussed in the ecological and evolutional contexts (Wheeler and Smith 2019; Wheeler et al., 2021). Our aglycone analysis unveiled that the three species share the same aglycones, likely synthesized via a flavonoid biosynthesis pathway proposed in Fig. 3; but, the proportion differed in the three *Puya* species. It means that the regulation in the biosynthesis of flavonoid causes the different coloration in these flowers. The inter-specific difference in the proportion of the myricetin and tricetin types implies that the biosynthetic genes of flavonoid 3',5'-hydroxylase (F3'5'H) are one of the key providing the color variations.

Pale-yellow flower coloration due to flavonols is unusual (Hashimoto et al., 2008; Iwashina et al., 1988). It has been mainly known to be attributed by 6- or 8-hydroxtylated yellow flavonols, chelated with alum, or under relatively high pH conditions in vacuole (Mishio et al., 2006; Stewart et al., 1975; Harborne 1968; Tanikawa et al., 2008). The turquoise petal of *P. alpestris* and pale-yellow *P. chiliensis* had relatively high pH 6.2 and 6.0, respectively. On the other hand, the pH of bluish flowered *P. coerulea* var. *violacea*, was general pH 5.2. We propsed that relatively high vacuolar pH is adaptive in pale-yellow and turquoise flowers of *Puya* species.

It has been known that the subtle pH differences cause great changes in the absorption spectrum of flower pigments (Stavenga et al., 2021). In addition, it has been suggested that the floral spectral properties are tuned to optimize their visibility to pollinators as an advertisement (Stavenga et al., 2021; van der Kooi 2021). The visual modeling of the flower color reconstructed by pigments *in vitro* demonstrated the effect of pH-dependent color changes on avian visual perceptions (Figs. 4, 5 and 6). In both of UVS- and VS-avian color spaces, similar pH-depending changes were observed on Δ*S* and spectral purity values. By increasing pH from 5.0 to 7.0, the values largely increased in **11** and **1 + 8 + 11**, especially in the UVS-avian color space. The effect of pH seemed relatively small for VS-birds. The high vacuolar pH in *P. alpestris* (pH 6.2) and *P. chilensis* (pH 6.2) would contribute to increase the floral Δ*S* and spectral purity, being conspicuous to UVS-birds rather than VS-birds. The most frequent visitors to *P. alpestris* and *P. chilensis* are the Chilean mockingbird, *Mimus thenca* (Hornung-Leoni et al., 2013), whose visions is considered to be UVS-type (Ödeen et al., 2011). The unusual high pH of *P. alpestris* and *P. chilensis* may be an adaptive trait to attract UVS-birds. On the other hand, no significant difference was detected in **1 + 8** between the two pH. In blue *P. coerulea* var. *violacea* (pH 5.2), to which the VS-type giant hummingbird *Patagona gigas* frequently visit (Hornung-Leoni et al., 2013), its color parameters Δ*S*, Δ*L* and spectral purity may not be affected by pH at least in the range of 5–7.

In this study, we compared the coloration at different pH using **1**, **8** and **11**, which have been shown as pigments responsible for the turquoise coloration in a previous study (Mizuno et al., 2021). Nevertheless,

we isolated and identified 16 compounds from petals; there might be more complex relationship between flower color, pigments, and pH in nature. Reflectance spectral data of intact petals would be also of importance for understanding the color characteristics. We will conduct further studies.

Specialized metabolites attract pollinators as multiple stimuli including a visual cue, and their vast diversity has been shown (Harborne and Smith, 1978; Mori et al., 2023). The glycosylation and acylation of anthocyanins cause the modification of its absorption spectrum (Giusti et al., 1999; Mazza and Brouillard, 1987). Furthermore, the spectral shifts also can be occurred by the presence of accessory pigments (Mazza and Brouillard, 1990; Trouillas et al., 2016). We need to address this diversity to understand plant-pollinator interactions (Wong et al., 2023). In this study, we first applied the pollinator visual modeling for isolated pigments, which may be an effective tool for ecological and evolutionary studies of plant-pollinator interactions. The modeling of *in vitro* reconstructed color provides the additional perspective to chemical studies of flower pigments.

Conclusion

Phylogenetic studies of the Chilean *Puya* species have suggested that the turquoise flowered *P. alpestris* is a hybrid between the blue and pale-yellow *Puya* species (Jabaily and Sytsma, 2010; Jabaily and Sytsma, 2013). This study revealed that the chemical structures of flavonoids and their distribution in the different flower colored Chilean *Puya* species, i.e., blue *P. coerulea* var. *violacea*, turquis *P. alpestris*, and pale-yellow *P. chilensis*. The flavonoid composition of *P. alpestris* without anthocyanin is essentially intermediate between blue and pale-yellow flowered species, which is congruent with the molecular phylogeny. The visual modeling using reconstructed flower color with the isolated compounds suggested that relatively higher pH of *P. alpestris* and *P. chiliensis* flowers is an adaptive trait to their UVS-bird pollinators. We propose that the turquoise color expression of *P. alpestris* is caused by regulation of the pH and flavonoid composition. Further analysis might be needed for understanding of the variation of flower colors of Chilean *Puya* species.

Experimental

Plant material

Fresh petals of *Puya coerulea* var. *violacea* (Brongn.) (16.0 g) were collected from the Tsukuba Botanical Garden, National Museum of Nature and Science (Tsukuba, Japan) in March 2019. Fresh petals of *P. chilensis* Molina (21.0 g) were collected from the Atagawa Banana Wani-en (Shizuoka, Japan) in March 2021. Fresh petals of *P. alpestris* (Poepp.) Gay (ca. 10 g) were collected from the Botanical Gardens of Osaka Metropolitan University (Osaka, Japan) in June 2019. Tip side of the petals was used for the measurement of UV–vis absorption spectra, HPLC analysis and pH measurement.

Isolation and identification of the anthocyanins, flavonols and flavones

Fresh petals of each species were extracted using 5% HCOOH in MeOH. After removing solvents by evaporation, each extract was applied to column chromatography using Diaion HP-20SS (Mitsubishi Chemical Co., Japan) and eluted with 0.5% TFA (trifluoroacetic acid), 10% MeCN containing 0.5% TFA and 25% MeCN containing 0.5% TFA. The fractions were chromatographed on a Sephadex LH-20 gel, eluenting with MeOH/H_2O/HCOOH (70:25:5). The mixtures were applied to preparative HPLC using a Shimadzu HPLC system equipped with an Inertsil ODS-4 column (I.D. 10 × 250 mm, GL Sciences Inc., Japan) under the following conditions. The eluent was 10% MeCN containing 5% HCOOH to 20% MeCN containing 5% HCOOH at a flow rate of 3 – 3.5 mL min^{-1}.

Three anthocyanins (**1**–**3**), four flavonols (**4**–**7**), and three flavones (**8**–**10**) were isolated from *P. coerulea* var. *violacea*, and three flavonols (**11**, **12** and **14**) and three flavones (**13**, **15** and **16**) were from *P. chilensis*. They were characterized by UV–vis spectroscopy, wavelength at 400–700 nm for anthocyanins, and 220–500 nm for the other flavonoids (Mabry et al., 1970), liquid chromatography-mass spectrometry (LC/MS) and nuclear magnetic resonance (NMR), and HPLC and TLC comparisons with authentic specimens. The origins of the authentic specimens were as follows: delphinidin 3,3',5'-tri-*O*-glucoside, apigenin and luteolin 4'-*O*-glucosides, and myricetin 3-*O*-rutinoside-3',5'-di-*O*-glucoside and 3,3',5'-tri-*O*-glucoside from the flowers of *P. alpestris* (Mizuno et al., 2021), quercetin 3,3'-*O*-glucoside was obtain from partial hydrolysis of **4**, delphinidin 3-*O*-glucoside and quercetin 3-*O*-rutinoside (rutin) from Funakoshi Co., Ltd. (Tokyo, Japan), and isorhamnetin 3-*O*-rutinoside from the leaves of *Saussurea pricei* N.D.Simpson (Asteraceae) (Kusano et al., 2010).

The MS was performed on a Shimadzu LC/MS system using an Inertsil ODS-4 column (I.D. 10×250 mm, GL Sciences Inc., Tokyo) equipped with a PDA detector (4.5 kV for ESI^+ and 3.5 kV for ESI^-; interface temperature as 250°C).

NMR spectroscopy was recorded on a Bruker AVANCE III HD 800 spectrometer equipped with a 5-mm TCI cryogenic probe and Z-axis gradient (Bruker Biospin AG, Switzerland). All spectra were obtained in 0.6 mL of the deuterated solvent placed inside 5-mm NMR tubes (Wilmad Lab Glass, USA) at 298 K. The compounds of **4** and **12**–**16** were dissolved in CD_3OD as the NMR solvent. Chemical shifts are reported in ppm and referenced to the residual methanol peaks observed at δ_H = 3.31 and δ_C = 49.00. Standard Bruker pulse sequences were employed. All NMR data reported were obtained via 1D ^1H and ^{13}C NMR, 2D ^1H DQF-COSY, 2D ^1H NOESY (mixing time = 400, 500, or 750 ms), 2D $^1H\{^{13}C\}$ edited-HSQC, 2D $^1H\{^{13}C\}$ HMBC, and 2D $^1H\{^{13}C\}$-HMQC-COSY experiments. Data analyses were performed using Bruker TopSpin software (v. 3.5; Bruker Biospin AG, Switzerland).

HPLC comparisons

The fresh petals were extracted with MeOH containing 5% HCOOH. The extract was filtered through a 0.45 μm GL Chromatodisk filter 13N (GL Sciences Inc.) and then subjected to HPLC. HPLC analysis was performed on a Shimadzu HPLC system equipped with an SPD-20A UV-vis detector (Shimadzu) using a InertSustain C18 column (I.D. 4.6 × 250 mm, GL Sciences Inc.) at a flow rate of 1.0 mL min^{-1}. The mobile

phase consisted of solvent A (5% HCOOH aq.) and solvent B (90% MeCN containing 5% HCOOH). The gradient solution program was as follows: linear gradient from 10 to 50% B for 35 min, followed by 50% B for 10 min. Flavonoid composition was compared among the three species with LCSolution software (Shimadzu).

Aglycone analysis

Aglycone analysis was performed according to Mizuno et al. (2020). Crude extracts (1 mL) from the three *Puya* species were added into 0.1 mL 12% aq. HCl, and treated for 40 min at 100°C. After cooling, the solutions were diluted with 4 mL water and applied to Sep-pak C18 cartridge (Waters) eluted with 2 mL H_2O, 2 mL 10% MeCN containing 0.5% TFA and 1 mL MeOH. The MeOH fractions were applied to HPLC (See section 5.4.). Authentic myricetin was purchased from Sigma, and quercetin, luteolin, apigenin and chrysoeriol was from Extrasynthese (France). Authentic kaempferol and isorhamnetin were isolated from the fruits of *Sophora japonica* L. and *Epiphyllum hybrida* (Cactaceae), respectively (Iwashina and Kondo 1985). Authentic laricitrin, tricetin and selagin were obtained by acid hydrolysis of **14**, **15** and **16**.

Absorption spectra

UV–vis absorption spectra (400–700 nm) of the petals of three *Puya* species were measured according to Mizuno et al. (2021) using a UV-2600 spectrophotometer (Shimadzu, Japan) equipped with an integrated sphere ISR-2600 (Shimadzu).

Chemical data of the compounds

Delphinidin 3,3',5'-tri-*O*-glucoside (**1**, Preternatin C5). TLC: R_f 0.03 (BAW), 0.02 (BuHCl), 0.38 (1% HCl), 0.57 (AHW); UV–vis: λ_{max} (nm) 0.01% HCl–MeOH 276, 522; E_{440}/E_{max} 32%; +$AlCl_3$ no change; LC-MS: *m/z* 789 $[M]^+$, 627 $[M - 162]^+$, 303 $[M - 162\times3]^+$.

Delphinidin 3',5'-di-*O*-glucoside (**2**). TLC: R_f 0.08 (BAW), 0.02 (BuHCl), 0.07 (1% HCl), 0.29 (AHW); UV–vis: λ_{max} (nm) 0.01% HCl–MeOH 278, 532; E_{440}/E_{max} 27%; +$AlCl_3$ no change; LC-MS: *m/z* 627 $[M]^+$, 303 $[M - 162\times2]^+$.

Delphinidin 3-*O*-glucoside (**3**). TLC: R_f 0.13 (BAW), 0.02 (BuHCl), 0.03 (1% HCl), 0.10 (AHW); UV–vis: λ_{max} (nm) 0.01% HCl–MeOH 278, 543; E_{440}/E_{max} 21%; +$AlCl_3$ bathochromic shift; LC-MS: *m/z* 465 $[M]^+$, 303 $[M - 162]^+$.

Quercetin 3-*O*-rutinoside-3'-*O*-glucoside (**4**). TLC: R_f 0.47 (BAW), 0.64 (15% HOAc), 0.58 (BEW); Color under UV (365 nm): dark purple, UV/NH_3: yellow; UV: λ_{max} (nm) MeOH 266, 349; +NaOMe 276, 324, 398 (inc.); +$AlCl_3$ 274, 302, 354, 393; +$AlCl_3$/HCl 275, 302, 349, 393; +NaOAc 273, 328, 399; +NaOAc/H_3BO_3 267, 354; LC-MS: *m/z* 627 $[M + H - 146]^+$, 303 $[M + H - 162\times2 - 146]^+$, 771 $[M - H]^-$. ^1H and ^{13}C NMR data, see Table 2.

Quercetin 3,3'-di-*O*-glucoside (**5**). TLC: R_f 0.59 (BAW), 0.50 (15% HOAc), 0.68 (BEW); Color under UV (365 nm): dark purple, UV/NH_3: yellow. UV: λ_{max} (nm) MeOH 266, 346; +NaOMe 278, 324, 402 (inc.); +$AlCl_3$ 273, 303, 347, 390; +$AlCl_3$/HCl 273, 305, 352, 402; +NaOAc 272, 316, 397; +NaOAc/H_3BO_3 267, 353; LC-MS: *m/z* 625 $[M - H]^-$, 463 $[M - H-162]^-$.

Quercetin 3-*O*-rutinoside (**6**, rutin). TLC: R_f 0.69 (BAW), 0.49 (15% HOAc), 0.72 (BEW); Color under UV (365 nm): dark purple, UV/NH_3: yellow. UV: λ_{max} (nm) MeOH 259, 358; +NaOMe 276, 324, 413 (inc.); +$AlCl_3$ 274, 305, 325, 426; +$AlCl_3$/HCl 269, 299, 356, 396; +NaOAc 272, 306, 398; +NaOAc/H_3BO_3 262, 318, 379; LC-MS: *m/z* 303 $[M + H - 162 - 146]^+$, 609 $[M - H]^-$.

Isorhamnetin 3-*O*-rutinoside (**7**, narcissin). TLC: R_f 0.78 (BAW), 0.55 (15% HOAc), 0.84 (BEW); Color under UV (365 nm): dark purple, UV/NH_3: dark yellow. UV: λ_{max} (nm) MeOH 267, 350; +NaOMe 270, 329, 399 (inc.); +$AlCl_3$ 266, 296, 353; +$AlCl_3$/HCl 270, 298, 353; +NaOAc 268, 353; +NaOAc/H_3BO_3 267, 352; LC-MS: *m/z* 317 $[M + H - 162 - 146]^+$, 623 $[M - H]^-$.

Luteolin 4'-*O*-glucoside (**8**). TLC: R_f 0.73 (BAW), 0.11 (15% HOAc), 0.79 (BEW); Color under UV (365 nm): dark purple, UV/NH_3: dark purple. UV: λ_{max} (nm) MeOH 269, 336; +NaOMe 265, 296, 368 (dec.); +$AlCl_3$ 275, 293, 341, 387sh ; +$AlCl_3$/HCl 279, 296, 343, 387sh; +NaOAc 269, 337; +NaOAc/H_3BO_3 270, 337; LC-MS: *m/z* 449 $[M + H]^+$, 287 $[M + H - 162]^+$, 447 $[M - H]^-$.

Apigenin 4'-*O*-glucoside (**9**). TLC: R_f 0.81 (BAW), 0.19 (15% HOAc), 0.81 (BEW); Color under UV (365 nm): dark purple, UV/NH_3: dark purple. UV: λ_{max} (nm) MeOH 270, 326; +NaOMe 289, 354 (dec.); +$AlCl_3$ 291, 334, 386sh; +$AlCl_3$/HCl 291, 334, 375sh; +NaOAc 270, 325; +NaOAc/H_3BO_3 270, 327; LC-MS: *m/z* 433 $[M + H]^+$, 271 $[M + H - 162]^+$, 431 $[M - H]-$.

Tricetin 4'-*O*-glucoside (**10**). TLC: R_f 0.74 (BAW), 0.12 (15% HOAc), 0.77 (BEW); Color under UV (365 nm): dark purple, UV/NH_3: dark purple. UV: λ_{max} (nm) MeOH 271, 331; +NaOMe 274, 383 (dec.); +$AlCl_3$ 279, 335, 390sh; +$AlCl_3$/HCl 279, 300, 335, 387sh; +NaOAc 271, 333; +NaOAc/H_3BO_3 271, 333; LC-MS: *m/z* 463 $[M - H]^-$, 301 $[M - H-162]^-$.

Myricetin 3,3',5'-tri-*O*-glucoside (**11**). TLC: R_f 0.26 (BAW), 0.58 (15% HOAc), 0.37 (BEW); Color under UV (365 nm): dark purple, UV/NH_3: yellow. UV: λ_{max} (nm) MeOH 248, 267, 350; +NaOMe 278, 330, 400 (inc.); +$AlCl_3$ 275, 305sh, 354, 399; +$AlCl_3$/HCl 276, 305sh, 349, 396; +NaOAc 266, 322sh, 407; +NaOAc/H_3BO_3 266, 301sh, 362; LC-MS: *m/z* 643 $[M + H - 162]^+$, 481 $[M + H - 162\times2]^+$, 319 $[M + H - 162\times3]^+$, 803 $[M - H]^-$.

Myricetin 3,3'-di-*O*-glucoside (**12**). TLC: R_f 0.40 (BAW), 0.32 (15% HOAc), 0.52 (BEW); Color under UV (365 nm): dark purple, UV/NH_3: yellow. UV: λ_{max} (nm) MeOH 254, 297, 356; +NaOMe 275, 328, 412 (inc.); +$AlCl_3$ 273, 306, 425; +$AlCl_3$/HCl 273, 306, 357, 400; +NaOAc 269, 327, 410; +NaOAc/H_3BO_3 260, 306, 378; LC-MS: *m/z* 481 $[M + H - 162]^+$, 319 $[M + H - 162\times2]^+$,641 $[M - H]-$. ^1H and ^{13}C NMR data, see Table 2.

Tricetin 3',5'-di-*O*-glucoside (**13**). TLC: R_f 0.29 (BAW), 0.10 (15% HOAc), 0.37 (BEW); Color under UV (365 nm): dark purple, UV/NH_3: yellow. UV: λ_{max} (nm) MeOH 269, 340; +NaOMe 258, 330, 399 (inc.); +$AlCl_3$ 278, 299, 352, 385; +$AlCl_3$/HCl 279, 298, 347, 382; +NaOAc 259, 401; +NaOAc/H_3BO_3 267, 354, 398; LC-MS: *m/z* 627 $[M + H]^+$, 625 $[M - H]^-$, 311 $[M - H-162\times2]^-$. ^1H and ^{13}C NMR data, see Table 3.

Laricitrin 3,5'-di-*O*-glucoside (**14**). TLC: R_f 0.37 (BAW), 0.34 (15% HOAc), 0.59 (BEW); Color under UV (365 nm): dark purple, UV/NH_3: yellow. UV: λ_{max} (nm) MeOH 256, 267, 348; +NaOMe 275, 331, 401 (inc.); +$AlCl_3$ 274, 304, 358, 398; +$AlCl_3$/HCl 276, 300, 349, 393; +NaOAc 267, 360; +NaOAc/H_3BO_3 265, 328, 408; LC-MS: *m/z* 495 $[M + H - 162]^+$, 333 $[M + H - 162\times2]^+$, 655 $[M - H]^-$; ^1H and ^{13}C NMR data, see Table 2.

Tricetin 3'-*O*-glucoside (**15**). TLC: R_f 0.38 (BAW), 0.17 (15% HOAc), 0.56 (BEW); Color under UV (365 nm): dark purple, UV/NH_3: yellow. UV: λ_{max} (nm) MeOH 250, 265, 351; +NaOMe 271, 326, 407 (inc.); +$AlCl_3$ 271, 307, 356, 388; +$AlCl_3$/HCl 274, 423; +NaOAc 265, 330sh, 403; +NaOAc/H_3BO_3 258, 374; LC-MS: *m/z* 465 $[M + H]^+$, 463 $[M - H]^-$; ^1H and ^{13}C NMR data, see Table 3.

Selagin 5'-*O*-glucoside (**16**). TLC: R_f 0.47 (BAW), 0.21 (15% HOAc), 0.49 (BEW); Color under UV (365 nm): dark purple, UV/NH_3: yellow. UV: λ_{max} (nm) MeOH 269, 336; +NaOMe 275, 389 (inc.); +$AlCl_3$ 275, 305, 358, 392; +$AlCl_3$/HCl 278, 300, 348, 393; +NaOAc 262, 322; +NaOAc/H_3BO_3 266, 348, 404; LC-MS: *m/z* 479 $[M + H]^+$, 477 $[M - H]^-$; ^1H and ^{13}C NMR data, see Table 3.

Principal component (PC) analysis

The PC analysis was performed with the R (R Core Team, 2021) using HPLC chromatograms of the three *Puya* species. A total of 20 variables including flavones, flavonols and anthocyanins (Table 1), 17 variables including flavones and flavonols (Table 1), and ten variables in aglycone analysis were used (Table S1).

Visual model of pollinators and color variables using the isolated compound

The petal tips of two *Puya* species, *P. coerulea* var. *violacea* and *P. chilensis*, were homogenized to obtain the pressed juice. pH of the juice was immediately measured on three independently pressed juice for each species, using a twin pH meter AS-212 (HORIBA, Japan). The pH in the petal tips of *P. alpestris* refers to our previous study (Mizuno et al., 2021).

The flower color of the three *Puya* species was modeled and reconstructed with 0.07 mM **1** + 0.1 mM **8** (**1 + 8**) for *P. coerulea* var. *violacea*, 0.07 mM **1** + 0.1 mM **8** + 0.1 mM **11** (**1 + 8 + 11**) for *P. alpestris*, and 0.1 mM **11** (**11**) for *P. chilensis*. Each solution was prepared at pH 5.0 and 7.0 in Mcilvaine buffer. The reflectance spectra (300–750 nm) of the solutions were measured on a UV-2600 spectrophotometer (Shimadzu) equipped with an integrated sphere ISR-2600 (Shimadzu) using a D30 cell, divided by center partition (GL Sciences Inc., Japan). Ba_2SO_4 powder was used as a white standard.

The color loci of each solution in the pollinator's perceptual color space were computed based on their diffuse reflectance spectra with the R v. 4.1.2 (R Core Team, 2021) package *pavo* v. 2.7.0 (Maia et al., 2019). To model the vision of avian pollinators, the color loci were projected in the tetrahedron vision space (Endler and Mielke, 2005). Since floral visitors of *P. coerulea*, *P. alpestris* and *P. chilensis* (Hornung-Leoni et al., 2013) include both UVS- and VS-type (Ödeen and Håstad, 2010), the calculations were performed with the spectral sensitivity of both UVS- and VS-avian (Maia et al., 2019). The CIE D65 daylight irradiance spectrum was used as a model of daylight irradiance. Averaged reflectance spectrum of leaves in *pavo* was assumed as the background.

The distance from the flower locus to the tetrahedron achromatic center was calculated as spectral purity (Stoddard and Prum, 2011). Achromatic (ΔL) and chromatic contrasts (ΔS) against a leaf background were calculated in the receptor noise-limited model (RNL model; Vorobyev and Osorio, 1998). ΔL was calculated based on the double cone responsible for chromatic processing, according to Siddiqi et al. (2004). ΔS was obtained by weighting the Euclidean distance of the photoreceptor quantum catches by the Weber fraction of the cones. The Weber fraction (ω) was assumed to be 0.1 in the LWS mechanism, based on the empirically estimated value from the Pekin robin (*Leiothrix lutea*) (Maier, 1992; Olsson et al., 2018). Photoreceptor abundance of the cone types was estimated to be 1:2:2:4 for the UVS:SWS:MWS:LWS, according to those of *L. lutea* (Vorobyev and Osorio, 1998). ΔS was expressed in just noticeable difference (JND), where 1 JND is the theoretical threshold of color discrimination for stimuli viewed simultaneously under ideal viewing conditions (Vorobyev et al., 2001).

Statistical analyses were performed with R v. 4.1.2 (R Core Team, 2021). Significant differences among species were tested by one-way analyses of variance (ANOVA), using the *multcomp* package. The ANOVA was followed by a Tukey–Kramer post-hoc analysis to test the pairwise comparisons. $p < 0.05$ was considered statistically significant.

Declarations

Acknowledgements

The authors are grateful to Hideo Shimizu, Atagawa Tropical & Alligator Garden, Japan, Dr. Chie Tsutsumi, Tsukuba Botanical Garden, National Museum of Nature and Science, Japan, and some staffs for offering the flowers of living collections. The authors are grateful to Professor, Dr. Naonobu Noda, National Agriculture and Food Research Organization, Tsukuba-City, Ibaraki, Japan for useful advice. This work was supported by JSPS KAKENHI Grant Number 22K05643.

Competing interests: No competing interests exist

References

1. Buckingham J, Munasinghe V R N (2015) Dictionary of Flavonoids with CD-ROM. CRC.Press, Florida.

2. Harborne J B (1968) Comparative biochemistry of the flavonoids—VII: Correlations between flavonoid pigmentation and systematics in the family Primulaceae. Phytochemistry 7: 1215–1230 https://doi.org/10.1016/S0031-9422(00)85616-2
3. Harborne J B, Smith D M (1978) Correlations between anthocyanin chemistry and pollination ecology in the Polemoniaceae. Biochem Syst Ecol 6: 127–130 https://doi.org/10.1016/0305-1978(78)90038-8
4. Hashimoto M, Iwashina T, Kitajima J, Matsumoto S (2008) Flavonol glycosides from *Clematis* cultivars and taxa, and their contribution to yellow and white flower colors. Bull Nat Mus Nat Sci Ser B 34: 127–134
5. Hornung-Leoni C T, González-Gómez P L, Troncoso A J (2013) Morphology, nectar characteristics and avian pollinators in five Andean *Puya* species (Bromeliaceae). Acta Oecol 51: 54–61 https://doi.org/10.1016/j.actao.2013.05.010.
6. Iwashina T, Norio K (1985) Pigment components in the fruits of *Epiphyllum oxypetalum* (Cactaceae). Sci Rep Res Inst Evolut Biol 2: 119–123.
7. Iwashina T, Ootani S, Hayashi K (1988) On the pigmented spherical bodies and crystals in tepals of Cactaceous species in reference to the nature of betalains or flavonols. Bot Mag, Tokyo 101: 175–184
8. Iwashina T (2015) Contribution to flower colors of flavonoids including anthocyanins: a review. Nat Prod Commun 10: 529–544 1934578X1501000335.
9. Jabaily R S, Sytsma K J (2010) Phylogenetics of *Puya* (Bromeliaceae): placement, major lineages, and evolution of Chilean species. Amer J Bot 97: 337–356. https://doi.org/10.3732/ajb.0900107
10. Jiménez-Aspee F, Theoduloz C, Gómez-Alonso S, Hermosín-Gutiérrez I, Reyes M, Schmeda-Hirschmann G (2018) Polyphenolic profile and antioxidant activity of meristem and leaves from “chagual”(*Puya chilensis* Mol.), a salad from central Chile. Food Res Inter 114, 90–96. https://doi.org/10.1016/j.foodres.2018.07.051
11. Kandil F E, Grace M H, Seigler D S, Cheeseman J M (2004) Polyphenolics in *Rhizophora mangle* L. leaves and their changes during leaf development and senescence. Trees 18: 518–528 https://doi.org/10.1007/s00468-004-0337-8
12. Kusano K, Iwashina T, Kitajima J, Mishio T (2007) Flavonoid diversity of *Saussurea* and *Serratula* species in Tien Shan mountains. Nat Prod Commun 2: 1121–1128. https://doi.org/10.1177/1934578X0700201115
13. Lamer E, Malcher E, Grimshaw J (1968). Identification of 3',4',5',5,7-pentahydroxyflavone and its 3'-monoglucoside. Tetrahedron Lett 9: 1419–1421 https://doi.org/10.1016/S0040-4039(01)98969-5
14. Mabry T J, Markham K R, Thomas M B (1970) The Systematic Identification of Flavonoids, Springer, New York.
15. Maia R, Gruson H, Endler J A, White T E (2019) pavo 2: New tools for the spectral and spatial analysis of colour in R. Methods Ecol Evol 10: 1097–1107.

16. Maier E J (1992) Spectral sensitivities including the ultraviolet of the passeriform bird *Leiothrix lutea*. J Comp Physiol A, 170: 709–714 https://doi.org/10.1007/BF00198981.
17. Markham K R, Whitehouse L A (1984) Unique flavonoid glycosides from the New Zealand white pine, *Dacrycarpus dacrydioides*. Phytochemistry 23: 1931–1936 https://doi.org/10.1016/S0031-9422(00)84944-4
18. Markham K R, Geiger H (1994) ^{1}H Nuclear magnetic resonance spectroscopy of flavonoids and their glycosides in hexadeuterodimethylsulfoxide. In: Harborne J B (ed.), The Flavonoids: Advances in Research since 1986, pp. 441–498. Chapman & Hall, London.
19. Mishio T, Honma T, Iwashina T (2006) Yellow flavonoids in *Centaurea ruthenica* as flower pigments. Biochem Syst Ecol 34: 180–184 https://doi.org/10.1016/j.bse.2005.07.019
20. Mizuno T, Yangzom R, Devkota H P, Murai Y, Dorji R, Dorji K, Wangmo C, Gyeltshen C, Iwashina T (2020). Flavonol glycosides from the whitish flowers of *Primula alpicola* and *P. sikkimensis* var. *hopeana* in Bhutan. Bull Nat Mus Nat Sci Ser B, 46: 185–194.
21. Mizuno T, Sugahara K, Tsutsumi C, Iino M, Koi S, Noda N, Iwashina T (2021) Identification of anthocyanin and other flavonoids from the green–blue petals of *Puya alpestris* (Bromeliaceae) and a clarification of their coloration mechanism. Phytochemistry 181: 112581. https://doi.org/10.1016/j.phytochem.2020.112581
22. Mori S, Hasegawa Y, Moriguchi Y (2023) Color strategies of camellias recruiting different pollinators. Phytochemistry 207: 113559 https://doi.org/10.1016/j.phytochem.2022.113559
23. Ödeen A, Håstad O (2010) Pollinating birds differ in spectral sensitivity. J Comp Physiol A 196: 91–96 https://doi.org/10.1007/s00359-009-0474-z
24. Ödeen A, Håstad O, and Alström P (2011) Evolution of ultraviolet vision in the largest avian radiation-the passerines. BMC Evol Biol 11: 1–8 http://dx.doi.org/10.1186/1471-2148-14-62
25. Okitsu N, Noda N, Chandler S, Tanaka Y (2018) Flower color and its engineering by genetic modification. Ornamental Crops, 29–62
26. Olsson P, Lind O, Kelber A (2018) Chromatic and achromatic vision: parameter choice and limitations for reliable model predictions. Behav Ecol 29: 273–282 https://doi.org/10.1093/beheco/arx133
27. R Core Team, 2021. R: A language and environment for statistical computing. R Foundation for Statistical Computing, Vienna, Austria. https://www.R-project.org/.
28. Reynauld, J., Ismaili, A., & Jay, M. (1981). Flavonoid glycosides of *Lathyrus pratensis* leguminosae. Phytochemistry 20: 2052–2053 https://doi.org/10.1016/0031-9422(81)84073-3
29. Schulte K, Silvestro D, Kiehlmann E, Vesely S, Novoa P, Zizka G (2010) Detection of recent hybridization between sympatric Chilean *Puya* species (Bromeliaceae) using AFLP markers and reconstruction of complex relationships. Mol Phyl Evolut 57: 1105–1119 https://doi.org/10.1016/j.ympev.2010.09.001.
30. Scogin R, Freeman C E (1984) Floral pigments and nectar constituents in the genus *Puya* (Bromeliaceae). Aliso: J Syst Evolut Bot 10: 617–619

31. Scogin R (1985) Floral anthocyanins in the genus *Puya*. Biochem System Ecol 13: 387–389 https://doi.org/10.1016/0305-1978(85)90082-1.
32. Siddiqi A, Cronin T W, Loew E R, Vorobyev M, Summers K (2004) Interspecific and intraspecific views of color signals in the strawberry poison frog *Dendrobates pumilio*. J Exp Biol 207: 2471–2485 https://doi.org/10.1242/jeb.01047
33. Stavenga D G, Leertouwer H L, Dudek B, Van der Kooi C J (2021) Coloration of flowers by flavonoids and consequences of pH dependent absorption. Front Plant Sci 11: 600124 https://doi.org/10.3389/fpls.2020.600124
34. Stewart R N, Norris K H, Asen S (1975) Microspectrophotometric measurement of pH and pH effect on color of petal epidermal cells. Phytochemistry 14: 937–942 https://doi.org/10.1016/0031-9422(75)85162-4
35. Stoddard M C, Prum R O (2011) How colorful are birds? Evolution of the avian plumage color gamut. Behav Ecol 22: 1042–1052 https://doi.org/10.1093/beheco/arr088
36. Tanikawa N, Kashiwabara T, Hokura A, Abe T, Shibata M, Nakayama M (2008) A peculiar yellow flower coloration of *Camellia* using aluminum-flavonoid interaction. J Jap Soc Hort Sci 77: 402–407 https://doi.org/10.2503/jjshs1.77.402
37. Trouillas P, Sancho-García J C, De Freitas V, Gierschner J, Otyepka M, Dangles O (2016) Stabilizing and modulating color by copigmentation: Insights from theory and experiment. Chem. Rev 116: 4937–4982.
38. van der Kooi C J, Stavenga D G, Arikawa K, Belusic G, Kelber A (2021) Evolution of insect colour vision – from spectral sensitivity to visual ecology. Ann Rev Entomol 66: 435–461 https://doi.org/10.1146/annurev-ento-061720-071644
39. Vorobyev M, Osorio D (1998) Receptor noise as a determinant of colour thresholds. Proc Royal Soc B 265: 351–358 https://doi.org/10.1098/rspb.1998.0302.
40. Vorobyev M, Brandt R, Peitsch D, Laughlin S B, Menzel R (2001) Colour thresholds and receptor noise: behaviour and physiology compared. Vis Res 41: 639–653 https://doi.org/10.1016/S0042-6989(00)0028
41. Wheeler L C, Smith S D (2019) Computational modeling of anthocyanin pathway evolution: biases, hotspots, and trade-offs. Int Comp Biol 59: 585–598 https://doi.org/10.1093/icb/icz049
42. Wheeler L C, Wing B A, Smith S D (2021) Structure and contingency determine mutational hotspots for flower color evolution. Evolution Lett 5: 61–74 https://doi.org/10.1002/evl3.212
43. Williams C A (1978) The systematic implications of the complexity of leaf flavonoids in the Bromeliaceae. Phytochemistry 17: 729–734 https://doi.org/10.1016/S0031-9422(00)94216-X
44. Wong D C, Pichersky E, Peakall R (2023) Many different flowers make a bouquet: Lessons from specialized metabolite diversity in plant–pollinator interactions. Curr Opin Plant Biol 73: 102332 https://doi.org/10.1016/j.pbi.2022.102332
45. Wu Y, Sun B, Huang J, Gao H, Wu L (2007) A new flavonoid glycoside from the seeds of *Fagopyrum tataricum*. Asian J Trad Med 2: 202–205

46. Zizka G, Schneider J V, Schulte K, Novoa P (2013) Taxonomic revision of the Chilean *Puya* species (Puyoideae, Bromeliaceae), with special notes on the *Puya alpestris* -*Puya berteroniana* species complex. Brittonia 65: 387–407 https://doi.org/10.1007/s12228-012-9290-9.
47. Zscheile F P, White Jr J W, Beadle B W, Roach J R (1942). The preparation and absorption spectra of five pure carotenoid pigments. Plant Physiol 17: 331

Tables

Tables 1 to 3 are available in the Supplementary Files section.

Figures

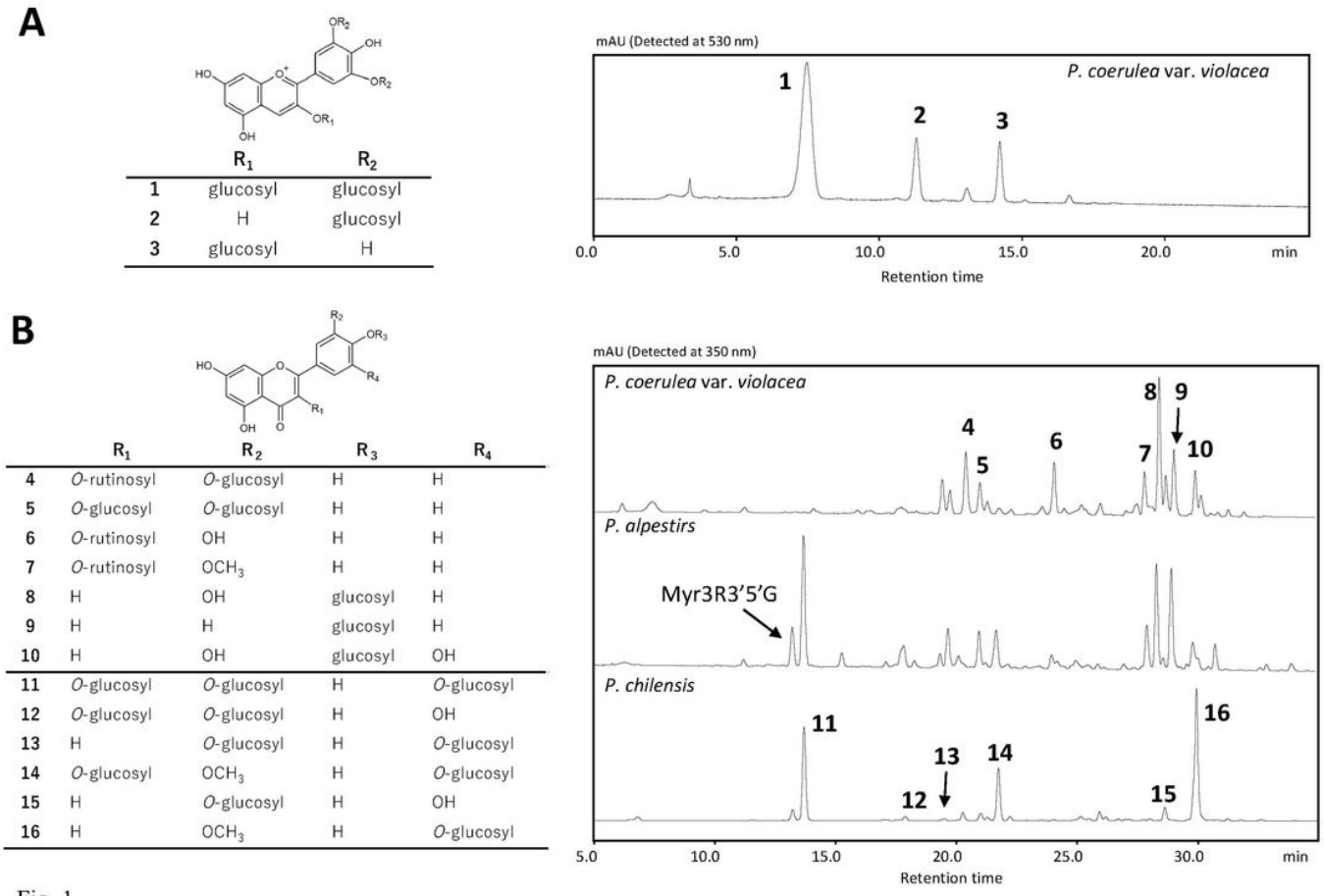

	R_1	R_2
1	glucosyl	glucosyl
2	H	glucosyl
3	glucosyl	H

	R_1	R_2	R_3	R_4
4	*O*-rutinosyl	*O*-glucosyl	H	H
5	*O*-glucosyl	*O*-glucosyl	H	H
6	*O*-rutinosyl	OH	H	H
7	*O*-rutinosyl	OCH_3	H	H
8	H	OH	glucosyl	H
9	H	H	glucosyl	H
10	H	OH	glucosyl	OH
11	*O*-glucosyl	*O*-glucosyl	H	*O*-glucosyl
12	*O*-glucosyl	*O*-glucosyl	H	OH
13	H	*O*-glucosyl	H	*O*-glucosyl
14	*O*-glucosyl	OCH_3	H	*O*-glucosyl
15	H	*O*-glucosyl	H	OH
16	H	OCH_3	H	*O*-glucosyl

Fig. 1.

Figure 1

The structure of isolated compounds, anthocyanins (**1**–**3**) (A), and flavonols (**4**–**7**,**11**, **12** and **14**) and flavones (**8**–**10**, **13**, **15** and **16**) (B), and their distributions in three Chilian *Puya* species by HPLC chromatograms (right side). **Myr3R3□5□G** = myricetin 3-*O*-rutinoside-3 ,5 -O-glucoside.

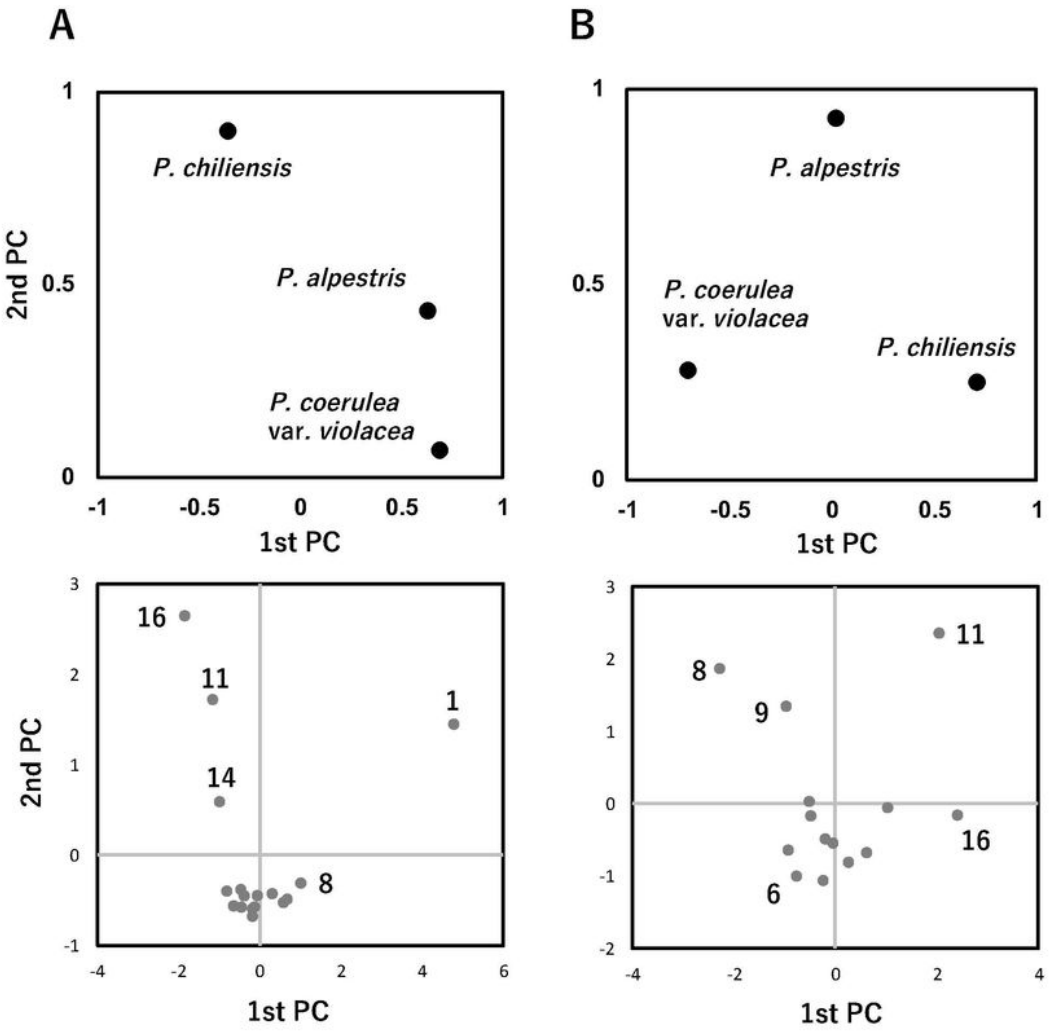

Fig. 2.

Figure 2

The scatter diagrams of the principal component analysis from the result of HPLC analysis of three Chilian *Puya* species including anthocyanin, flavone and flavonols, detected at 530 and 350 nm (a), and not including anthocyanins, detected only at 350 nm (b). The diagrams show the relationship among three Chilian *Puya* species (upper) and the relationship of respective compounds (lower).

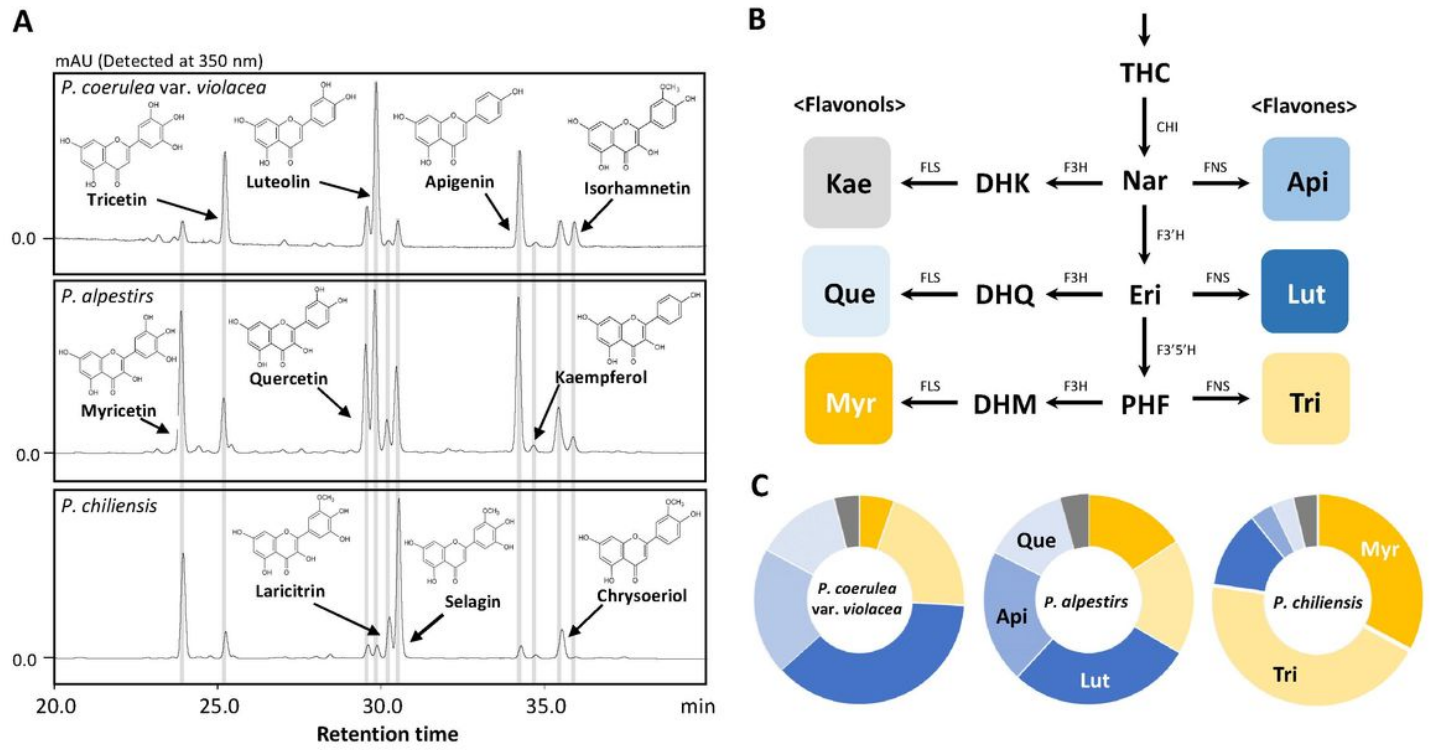

Fig. 3.

Figure 3

Aglycone analysis by HPLC in the three Chilian *Puya* species (A). Putative flavonoid biosynthesis and their related genes (B), and the proportion chart of the flavone and flavonol aglycones from the flower of three Chilian *Puya* species (C). THC = Tetrahydroxy chalcone, Nar = naringenin, Eri = Eriodictyol, PHF = Pentahydroxy flavanone, DHM = Dihydro myricetin, Api = apigenin, Lut = luteolin type flavones (luteolin and chrysoeriol), Tri = tricetin type flavones (tricetin and selagin), Qu = quercetin type flavonols (quercetin and isorhamnetin), Myr = myricetin type flavonols (myricetin and laricitrin). CHI = chalcone isomerase, F3H = flavanone 3-hydroxylase, F3 H = flavonoid 3 -hydroxylase, F3 5 H = flavonoid 3 ,5 -hydroxylase, FLS = Flavonol synthase, FNS = flavone synthase.

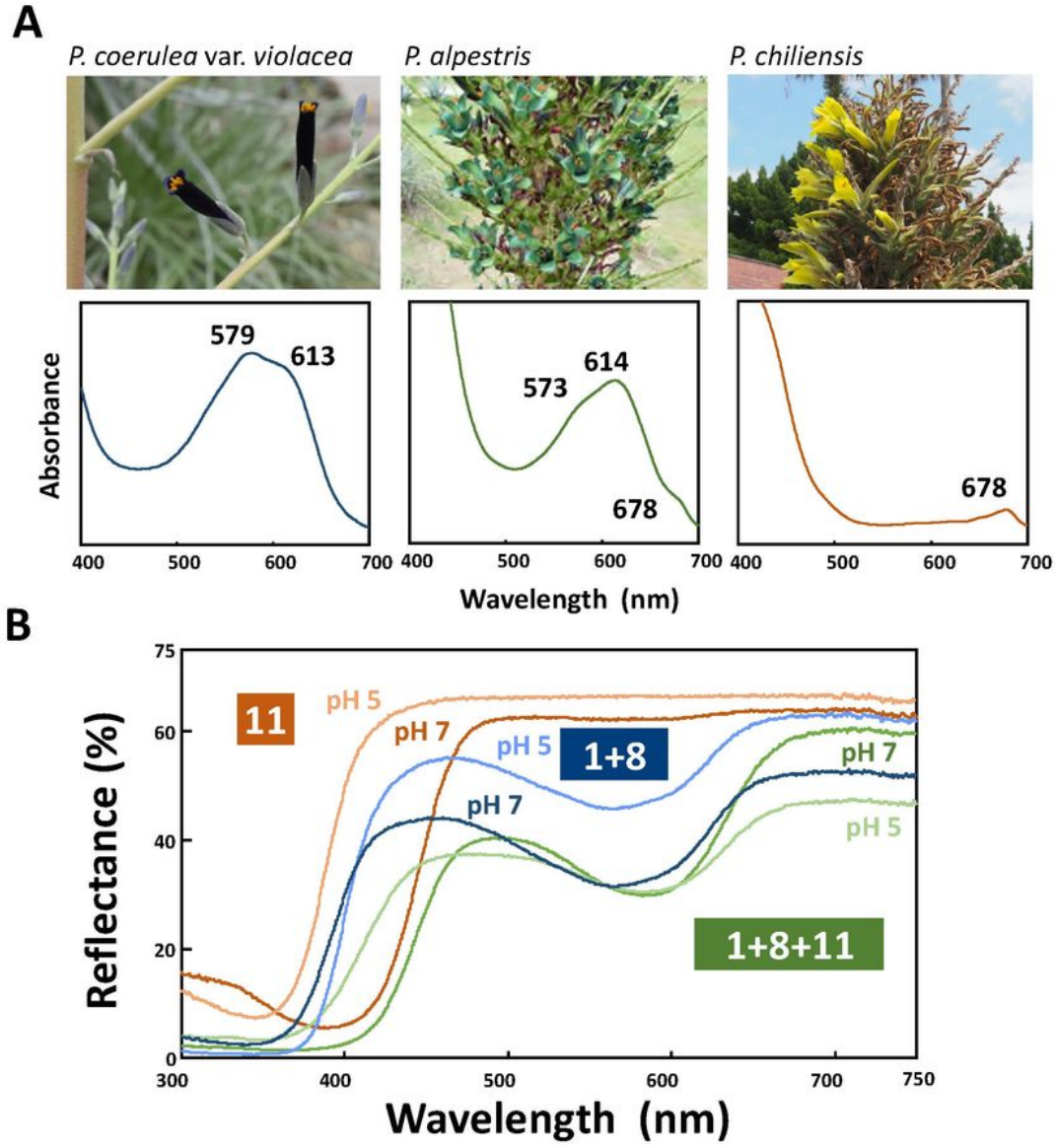

Fig. 4.

Figure 4

The visible absorption spectra of the flower of three Chilian *Puya* species (A), and their flowers photographed at Tsukuba Botanical Garden, National Museum of Nature and Science, Japan in March 2019 for the flower of *P. coerulea* var. *violacea*, Botanical Gardens of Osaka City University, Japan for the flower of *P. alpestris* in June 2021, and Atagawa Banana Wani-en, Japan in March 2021 for the flower of

P. chiliensis. Reflectance spectra of the isolated flavonol (0.1 mM **11**), the mixture of anthocyanin (0.07 mM **1**) and flavone (0.1 mM **8**), and the mixture of **1**, **8** and **11**(B).

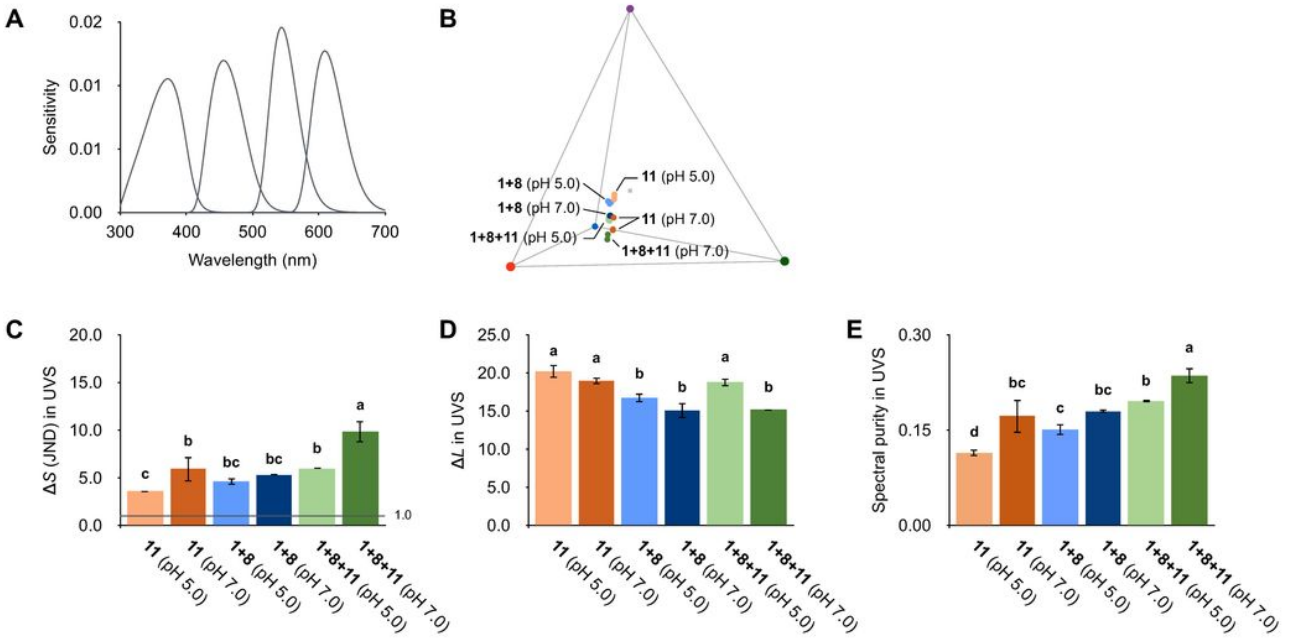

Figure 5

Visual modeling with the reconstructed solutions. Visual sensitivity curves of UVS-avian species (A). Color loci of petals plotted in the tetrahedral color spaces of UVS-avian species (B). Chromatic contrast (Δ*S*, C), achromatic contrast (Δ*L*, D) and spectral purity (E) of petals against foliage background in the UVS-avian species. The boxes in the center of the visual spaces indicate the achromatic center. The sensitivity curves were generated using the R (R Core Team, 2021) using *pavo* package 2.7.0 (Maia et al., 2019).

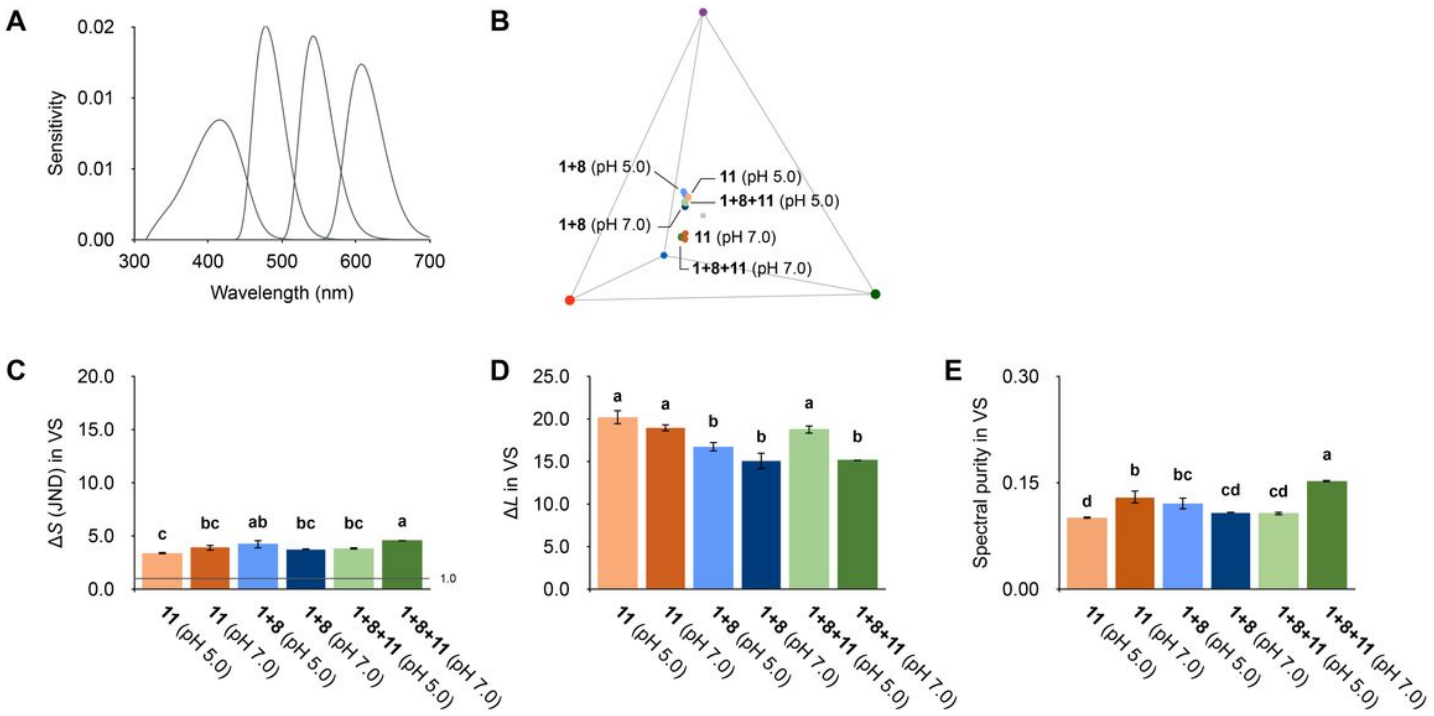

Figure 6

Visual modeling with the reconstructed solutions. Visual sensitivity curves of VS-avian species (A). Color loci of petals plotted in the tetrahedral color spaces of VS-avian species (B). Chromatic contrast (Δ*S*, C), achromatic contrast (Δ*L*, D) and spectral purity (E) of petals against foliage background in the VS-avian species. The boxes in the center of the visual spaces indicate the achromatic center. The sensitivity curves were generated using the R (R Core Team, 2021) using *pavo* package 2.7.0 (Maia et al., 2019).

Supplementary Files

This is a list of supplementary files associated with this preprint. Click to download.

- TableS1.PuyaJPRrvar3.xlsx
- FigSup.PuyaJPRver3.pptx
- Table1.PuyaJPRrvar3.xlsx
- Table2.PuyaJPRrvar3.xlsx
- Table3.PuyaJPRrvar3.xlsx